INORGANIC CHEMISTRY
FRONTIERS

http://rsc.li/frontiers-inorganic

INORGANIC CHEMISTRY
FRONTIERS

RESEARCH ARTICLE

(Boratabenzene)(cyclooctatetraenyl) lanthanide complexes: a new type of organometallic single-ion magnet†

Yin-Shan Meng,‡[a] Chun-Hong Wang,‡[b] Yi-Quan Zhang,[c] Xue-Bing Leng,[b] Bing-Wu Wang,*[a] Yao-Feng Chen*[b] and Song Gao*[a]

A series of new sandwich type lanthanide complexes containing both boratabenzene and cyclooctatetraenyl ligands, $[(C_5H_5BR)Ln(COT)]$ (**1Er**: R = H, Ln = Er; **2Er**: R = Me, Ln = Er; **3Er**: R = NEt₂, Ln = Er; **4Dy**: R = H, Ln = Dy; **5Dy**: R = Me, Ln = Dy; **6Dy**: R = NEt₂, Ln = Dy; **7Y**: R = NEt₂, Ln = Y), were synthesized. The structures of **1Er–7Y** were all characterized by single crystal X-ray diffraction. Dynamic susceptibility experiments showed that the erbium complexes **1Er–3Er** exhibited slow magnetic relaxation under zero dc field while the dysprosium complexes **4Dy–6Dy** did not. For the erbium complexes, the magnetic properties were influenced by the substituent on the boron atom. **1Er** exhibited hysteresis up to 8 K, and **2Er** featured the highest energy barrier (300 cm⁻¹) among all the reported erbium single-ion magnets (SIMs). The influence of the boron substituent on the magnetic properties was highlighted by *ab initio* calculations.

[a]*Beijing National Laboratory of Molecular Science, State Key Laboratory of Rare Earth Materials Chemistry and Applications, College of Chemistry and Molecular Engineering, Peking University, Beijing 100871, P. R. China. E-mail: wangbw@pku.edu.cn, gaosong@pku.edu.cn*
[b]*State Key Laboratory of Organometallic Chemistry, Shanghai Institute of Organic Chemistry, Chinese Academy of Sciences, 345 Lingling Road, Shanghai 200032, P. R. China. E-mail: yaofchen@mail.sioc.ac.cn*
[c]*Jiangsu Key Laboratory for NSLSCS, School of Physical Science and Technology, Nanjing Normal University, Nanjing 210023, P. R. China*
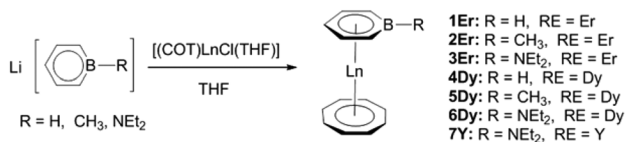†Electronic supplementary information (ESI) available. CCDC 1416019–1416025. For ESI and crystallographic data in CIF or other electronic format see DOI: 10.1039/c6qi00028b
‡These authors contributed equally to this work.

Introduction

Since the discovery of the Mn_{12} molecule which exhibits magnet-like behaviour at liquid helium temperature,[1] many efforts have been made to the design and synthesis of single-molecule magnets (SMMs).[2] This fascinating magnetic property originates from a combination of a large spin ground state and uniaxial magnetic anisotropy, and makes SMMs potential candidates for the next generation high-density data storage materials, quantum computing and spintronic devices.[3] Later, single-ion magnets (SIMs) which contain only a single spin carrier have been developed.[4] Recently, several reports disclosed that carbon-based ligands, such as Cp* and COT (Cp* = pentamethylcyclopentadienyl, COT = cyclooctatetraenyl), supporting erbium complexes show interesting SIM properties.[5]

Boratabenzenes are a type of heterocyclic, 6π-electron aromatic anion. The first boratabenzene derivative $[CpCoC_5H_5BPh]^+$ was reported by Herberich and co-workers in 1970.[6] One year later, Ashe III described the synthesis of lithium 1-phenylboratabenzene.[7] Their pioneering research opened up the fascinating area of boratabenzene chemistry. In the last four decades, a large number of metal complexes bearing boratabenzenes have been reported.[8,9] However, the properties and applications of these complexes were mostly limited to their reactivity and catalytic applications in organic and polymer synthesis.[10] Considering the similarity between boratabenzene and cyclopentadienyl, it is possible to construct new erbium SIMs by using boratabenzene ligands. On the other hand, boratabenzene is a poorer electron donor in comparison with Cp*, promoting the 4f electrons stretching along the uniaxial direction. Therefore, the uniaxial magnetic anisotropy of (boratabenzene)(cyclooctatetraenyl) lanthanide might be enhanced, which may bring a new opportunity in the design of erbium SIMs with high U_{eff} and/or T_B. Furthermore, the specific electrostatic contribution of boratabenzene and electronic structure modulation on SIMs can be tuned by the choice of the exocyclic substituent on boron. Herein, we report the synthesis, characterization and magnetic properties of (boratabenzene)(cyclooctatetraenyl) lanthanide complexes. The *ab initio* calculations were also performed to provide further insight into the magnetic properties of these complexes.

828 | *Inorg. Chem. Front.*, 2016, **3**, 828–835

This journal is © the Partner Organisations 2016

Results and discussion

Synthesis and structural characterization of (boratabenzene)(cyclooctatetraenyl) lanthanide complexes

Salt elimination reactions of $Li(C_5H_5BR)$ (R = H, Me, NEt_2) with $[(COT)LnCl(THF)]$ (Ln = Er, Dy, Y) in THF gave crude products, which recrystallized in toluene or hexane to provide the desired (boratabenzene)(cyclooctatetraenyl) lanthanide complexes $[(C_5H_5BR)Ln(COT)]$ (**1Er**: R = H, Ln = Er; **2Er**: R = Me, Ln = Er; **3Er**: R = NEt_2, Ln = Er; **4Dy**: R = H, Ln = Dy; **5Dy**: R = Me, Ln = Dy; **6Dy**: R = NEt_2, Ln = Dy; **7Y**: R = NEt_2, Ln = Y) in moderate yields (Scheme 1). Complexes **1Er–7Y** were characterized by single crystal X-ray diffraction. **1Er–7Y** all crystallize in the monoclinic space group $P2_1/c$. The molecular structures of **1Er–3Er** are shown in Fig. 1, while those of **4Dy–6Dy** and **7Y** are presented in the ESI.† The structural features of **1Er–3Er** and **4Dy–6Dy** are very similar and **1Er–3Er** were taken as the examples to analyze the structural features. **1Er–3Er** are sandwich type organometallic complexes, and the erbium ion is much closer to the centroid of the cyclooctatetraenyl ring (1.674–1.679 Å) than to that of the boratabenzene ring (2.245–2.257 Å). The average Er–C(COT) bond lengths in **1Er**, **2Er** and **3Er** are 2.495(8), 2.491(2) and 2.493(5) Å, respectively, which are close to that in $[(Cp^*)Er(COT)]$ (Cp^* = pentamethylcyclopentadienyl) (2.513 Å).[5a] On the other hand, the average Er–C(boratabenzene) bond lengths in **1Er**, **2Er** and **3Er** (2.661(8), 2.657(3) and 2.647(4) Å) are much longer than the average Er–C(Cp^*) bond length in $[(Cp^*)Er(COT)]$ (2.573 Å) as boratabenzene is a poorer electron donor in comparison with Cp^*. The Er–C(boratabenzene) bond lengths in **1Er**, **2Er** and **3Er** are in the ranges of 2.618(9)–2.694(9), 2.629(3)–2.678(3) and 2.603(8)–2.698(8) Å, respectively; the erbium ion is far away from the *ortho* carbon atoms and closer to the *para* carbon atom. The Er–B distances (2.76(1) Å (**1Er**), 2.779(3) Å (**2Er**) and 2.83(1) Å (**3Er**)) are longer than the Er–C(borata-benzene) distances. These observations revealed a slippage of the erbium ion away from boron and toward the *para* carbon. Due to the strong π-interaction between boron and the amino-substituent, the Er–B distance in **3Er** is longer than those in **1Er** and **2Er** and the deviation of the boron atom from the boratabenzene plane in **3Er** (0.097 Å) is larger than those in **1Er** and **2Er** (0.028 and 0.059 Å, respectively). Dihedral angles between the cyclooctatetraenyl ring and the boratabenzene ring in **1Er**, **2Er** and **3Er** are 10.6°, 5.5° and 9.3°, respectively. The nearest neighboring molecules are nearly perpendicular to each other through the C–H···B interaction and edge to face π···π stacking between the two aromatic rings. The nearest Er···Er distances in **1Er**, **2Er** and **3Er** are 6.1, 6.8 and 6.3 Å, respectively (see the ESI†).

Magnetic properties

Dc magnetic measurements were conducted under 1 kOe dc field with the temperature ranging from 300 to 2 K (Fig. 2 and S4 in the ESI†). At room temperature, the $\chi_m T$ values of **1Er**, **2Er**, **3Er**, **4Dy**, **5Dy** and **6Dy** are 11.01, 11.04, 11.08, 13.92, 13.94 and 14.06 emu mol^{-1} K, respectively, which are in good agreement with the theoretical values of Er^{III} ($^4I_{15/2}$, $S = 3/2$, $L = 6$, $g = 6/5$) and Dy^{III} ($^6H_{15/2}$, $S = 5/2$, $L = 5$, $g = 4/3$). The $\chi_m T$ value of **1Er** decreases very slightly with decreasing temperature, but when the temperature decreases to 12 K, the $\chi_m T$ value jumps to 11.32 cm^3 mol^{-1}, and then decreases sharply upon further cooling. The $\chi_m T$ value of **2Er** also slightly upturns at about 6 K, and then drops precipitously. Similar to other reported Er^{III} SIMs, upon a decrease of the temperature, the $\chi_m T$ value of **3Er** decreases slightly, until about 3 K where it drops drastically. The sudden drop in $\chi_m T$ observed for **1Er**, **2Er** and **3Er** indicated that their magnetizations are blocked. The sudden drop in $\chi_m T$ observed for **1Er**, **2Er** and **3Er** may arise from anti-ferromagnetic coupling, saturation of the magnetization, the Zeeman effect, and the spin–orbit coupling effect, which led to a change of spin population or magnetization blocking. This phenomenon is not uncommon in previously reported SMMs.[4f,5] The variable field dc measurements showed that the

Scheme 1 Synthesis of (boratabenzene)(cyclooctatetraenyl) lanthanide complexes.
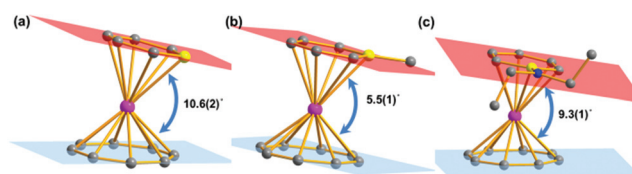

Fig. 1 Molecular structures of **1Er–3Er**. (a), (b) and (c) Represent **1Er**, **2Er** and **3Er**, respectively. Color code: pink, Er; dark grey, C; yellow, B; blue, N. Hydrogen atoms are omitted for clarity.
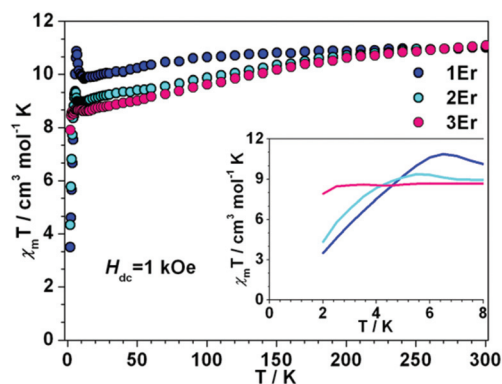

Fig. 2 Temperature dependence of the dc magnetic susceptibility time temperature $\chi_m T$ for **1Er–3Er** under 1 kOe applied magnetic field. (Inset) Expanded view of $\chi_m T$ vs. T plots below 8 K.

unusual $\chi_m T$ rising observed for **1Er** at 12 K is not due to the polycrystalline samples' reorientation along the magnetic field, but is related to the SIM properties (Fig. S5†). Further discussions on this $\chi_m T$ rising at low temperatures are provided *vide infra*. For Dy^{III} complexes, upon cooling, the $\chi_m T$ values are nearly constant until 100 K, and then slowly decrease. Below 25 K, the $\chi_m T$ values drop steeply upon further cooling. At 2 K, the values are 9.52, 10.00, and 10.00 emu mol^{-1} K, respectively (Fig. S4†). These static properties could be attributed to the typical stark sublevel depopulation.[11]

The out-of-phase ac susceptibility of **1Er** and **2Er** exhibited strong frequency-dependent behaviour between 15 K and 24 K or 16 K and 25 K under zero dc field (Fig. 3(a), (b) and S7, S8†), while below 10 K, no χ''_m peaks could be observed since the magnetic relaxation rate is so slow that it is beyond the lowest limit of our equipment (Fig. S9†). The relaxation time extracted from the temperature-dependent and frequency-dependent out-of-phase susceptibilities gave the same results (Fig. S10(a) and S10(b)†). The effective energy barrier of **1Er** is 371 K (259 cm^{-1}) with τ_0 of 5.3×10^{-12} s (Fig. 3(d)). The χ''_m peak of the 1 Hz plot for **2Er** is 17.4 K, which is higher than that for **1Er** (15.8 K) (Fig. 3(a), (b) and S7, S8†). As a consequence, the effective energy barrier and τ_0 of **2Er** are 421 K (300 cm^{-1}) and 5.5×10^{-12} s, respectively (Fig. 3(e)), whereas the τ *vs.* T^{-1} plot for **2Er** at low temperature showed an evident curvature, indicating a faster QTM process than that of **1Er**. The energy

barriers of **1Er** and **2Er** are higher than those of the previously reported erbium based SIMs (ranging from 15 cm^{-1} to 225 cm^{-1}),[4k,l,5] revealing the advantage of introducing poorer electron donating boratabenzene as the ligand. Utilizing a poorer electron donor decreases the electronic interaction between the 4f electrons and the aromatic electrons of ligands along the uniaxial direction, and enhances the uniaxial magnetic anisotropy. This experimental result is in line with the theoretical study of Rajaraman *et al.*[12] It is also noteworthy that **2Er** has the highest effective energy barrier among all reported Er^{III} SIMs. The out-of-phase ac susceptibility of **3Er** also showed strong frequency-dependent magnetic behaviour, which is significantly different from those observed for **1Er** and **2Er**. When the temperature is below 10 K, the intensity of the out-of-phase component of **3Er** is distinctly larger than those of **1Er** and **2Er**, implying a much stronger and faster QTM process. The peaks of the corresponding frequency plots are nearly unchanged until the temperature rises to 10 K, confirming the existence of a temperature independent QTM process (Fig. 3(c) and S11†). The effective energy barrier of **3Er** is 250 K (174 cm^{-1} under zero dc field) (Fig. 3(f) and S10(c)†). When an optimized field 2 kOe was applied, the U_{eff} increased slightly (Fig. 3(f) and S12†). The lower energy barrier of **3Er** compared to those of **1Er** and **2Er** can be attributed to two facts: (a) aminoboratabenzene is a better electron donor than the hydrogen (or methyl)-substituted one; (b) the deviation of the boron atom from the boratabenzene plane in **3Er** is larger than those in **1Er** and **2Er**, which may cause more transverse components (see *ab initio* calculations below). Dynamic studies showed that **4Dy–6Dy** only exhibited slow magnetic relaxation under an applied dc field with small effective energy barriers (Fig. S13–S15†). Combined with the previous reports, the sandwich type geometry utilizing cyclomultiene ligands seems not suitable for dysprosium to be a good SIM.

The hysteresis measurements showed that all Er^{III} complexes exhibited butterfly-type hysteresis loops (Fig. 4). Interestingly, **1Er** and **2Er** have the hysteresis loops up to 8 and 6 K, respectively, which are higher than that of [(Cp*)Er(COT)] (5 K).[5a] So far, only two Er^{III} complexes, [K(18-crown-6)(THF)$_2$][Er(COT)$_2$] (10 K),[5b–d] and [Li(DME)$_3$][Er(COT'')$_2$] (8 K),[5c] have blocking temperatures (T_B) up to 8 K, and both of them are ion pairs. For **3Er**, hysteresis could not be observed until the temperature was decreased to 2 K. To see whether thermal relaxation or QTM is predominant in T_B, we extrapolated the Arrhenius fitting and found that the blocking temperatures of **1Er–3Er** (defined as the relaxation time of 100 s) were similar, which were 12.8, 13.7 and 10.3 K, respectively. Therefore, hysteresis is mostly determined by the QTM rate and strength at low temperatures. The differences in their hysteresis we believe are due to the QTM, which could be caused by the following reasons: 1. the differences in their local structures. **2Er** has a smaller bending angle than **1Er**, which may be responsible for the observed higher U_{eff}, but the introduction of the electron-donating methyl group in **2Er** enhances the electronic interaction between the Er^{III} ion and the boratabenzene ligand along the uniaxial direction, leading to a more obvious QTM
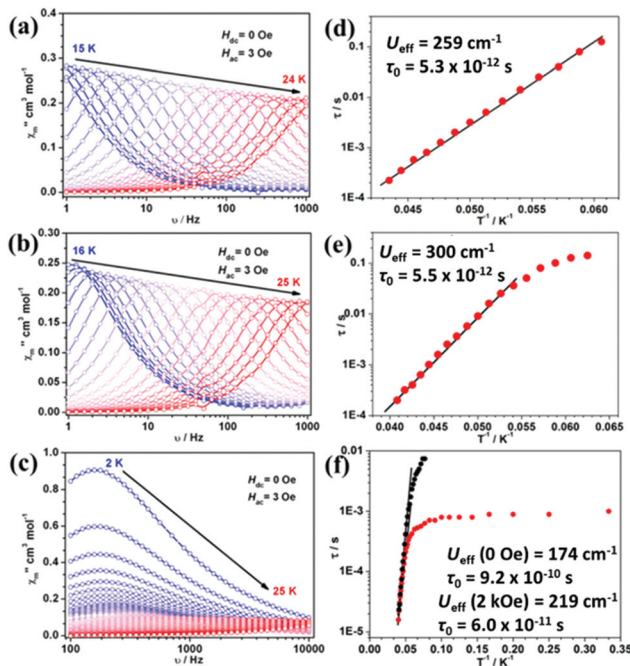
Fig. 3 Out-of-phase (χ''_m) signal *vs.* frequency (v) plots under 3 Oe ac field for **1Er** (a), **2Er** (b) and **3Er** (c). Relaxation time (τ) *vs.* inverse of temperature (T^{-1}) plots for **1Er** (d), **2Er** (e) and **3Er** (f). Red points were obtained under zero dc field while black points were obtained under 2 kOe dc field. The solid lines represent the fitting by applying the Arrhenius law.

830 | *Inorg. Chem. Front.*, 2016, **3**, 828–835

This journal is © the Partner Organisations 2016
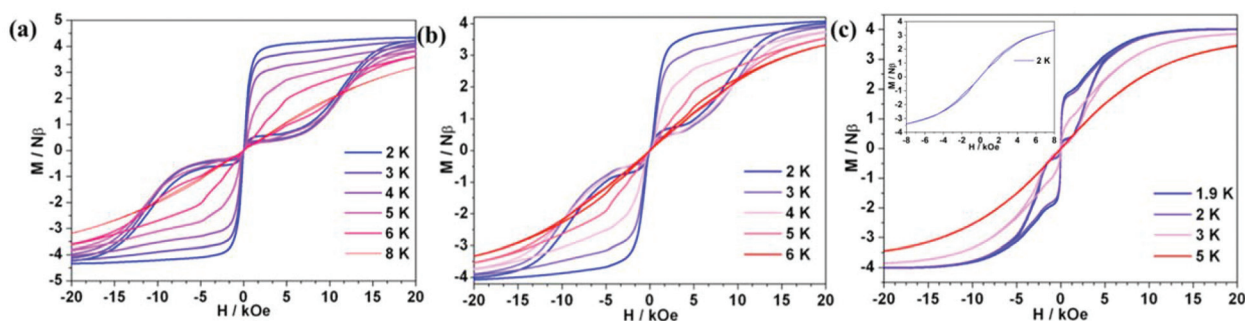
Fig. 4 Variable-field magnetization data for **1Er** (a), **2Er** (b), **3Er** (c inset) and diluted **3Er** (c) were collected at the average field sweeping rate of 1.9 mT s^{-1}. As a result of the QTM, the coercive field was not observed.

than that of **1Er**. For **3Er**, aminoboratabenzene is a better electron donor than the hydrogen (or methyl)-substituted one due to the strong π-interaction between boron and nitrogen. The π-interaction between boron and nitrogen also causes a deviation of the boron atom out from the 5 Cs plane of 0.097 Å, which is apparently larger than those in **1Er** and **2Er** (0.028 and 0.059 Å, respectively). The unchanged maximum of the out-of-phase ac susceptibility below 10 K for **3Er** implies a much stronger and faster QTM process compared to QTM of **1Er** and **2Er**. 2. As the dipole–dipole interaction is anisotropic, the different arrangement of molecules in the lattice may also give different QTM rates for **1Er**, **2Er** and **3Er**. Their different magnetic behaviors at low temperatures may also be caused by the different relaxation processes like the Direct/Raman process. Since QTM is more obvious in **3Er**, the dilution experiment was subsequently carried out to study the role of the dipole–dipole interaction. A diluted sample of **3Er** was prepared by the co-crystallization of **3Er** with the isostructural [[(COT) Y(C$_5$H$_5$BNEt$_2$)] in a Er : Y molar ratio of 1 : 19. The co-crystallization method has been used for the magnetic dilution studies of the analogues, such as [[Cp*)Er(COT)][5a] and [K(18-crown-6)(THF)$_2$][Er(COT)$_2$],[5b] by us and others. The ICP analysis indicated that the Er : Y molar ratio in the diluted sample is 4.2 : 95.8. The ac measurement indicated that the χ''_m peaks occur in the range of 18 to 26 K, with a U_{eff} of 239 cm^{-1}, which is higher than that of the pure **3Er** (174 cm^{-1}) under zero dc field (Fig. S16 and S17†). The variable-field magnetization plots displayed a hysteresis loop up to 3 K (Fig. 4(c)), which is still lower than those observed for **1Er** and **2Er**. The sudden magnetization loss near zero field still occurred and the coercive field was not observed. The above results indicated that the differences in the QTM of **1Er–3Er** are mainly due to their local structures.

Ab initio calculations

To further elucidate the differences in their dynamic relaxations, *ab initio* CASSCF/RASSI/SINGLE_ANISO calculations with the MOLCAS 7.8 package were performed to determine the low-lying energy levels and magnetic properties of molecules.[13]

The calculated results showed that the ground Kramer's doublets of Er^{III} complexes are well separated from the excited states (Table S3†). The effective g_z values of **1Er–3Er** are 17.87, 17.89 and 17.81, respectively, indicating their magnetically uniaxial anisotropic ground states. Correspondingly, the $g_{x,y}$ value is almost negligible ($g_{x,y} \approx 1 \times 10^{-4}$), except for **3Er** ($g_x$ = 0.0025, g_y = 0.0028). Even for the first excited Kramer's doublets, the transversal components still show small values for **1Er** and **2Er** ($g_{x,y} \approx 2 \times 10^{-2}$). A relatively opposite case happens for **3Er**, the $g_{x,y}$ value of the higher excited states increases obviously. These relatively large transverse components may promote a more pronounced QTM process, which is consistent with the hysteresis measurements. The calculations also revealed that all Dy^{III} complexes have small magnetic anisotropic ground Kramer's doublets and low energy first excited states (Table S4†). The $g_{x,y}$ values are not negligible, giving a significantly large transversal magnetic moment to Dy^{III} complexes. The energy gap between the ground state and the first excited state is also small. Fig. 5 indicates that the transversal diagonal magnetic moments (*ca.* 10$^{-1}\mu_B$) in the ground state arising from internal magnetic fields of **4Dy–6Dy** are much larger than those (*ca.* 10^{-3}–10$^{-4}\mu_B$) of **1Er–3Er**, therefore allowing a fast QTM. According to a recent proposal by Ungur and co-workers,[14] the relaxation path can be related to the tunneling gaps. Thus, according to the relaxation path indicated in Fig. 5, the blocking barriers of **1Er–6Dy** were deduced, which are 201.0 cm^{-1} (15/2− → 13/2− → 5/2+), 223.5 cm^{-1} (15/2− → 13/2− → 9/2− → 9/2+), 158.8 cm^{-1} (15/2− → 13/2− → 13/2+), 56.2 cm^{-1} (15/2− → 13/2− → 13/2+), 33.6 cm^{-1} (15/2− → 13/2+) and 39.7 cm^{-1} (15/2− → 11/2+), respectively. These calculated blocking barriers are in the same sequence of the experimental ones, although deviations in particular values are observed, due to the exclusion of electron dynamic correlation in the calculations. The tunneling gaps of the diagonal and off-diagonal in the ground and the first excited states of **3Er** are much larger than those of **1Er** and **2Er**, therefore **3Er** has the fastest QTM among the three Er^{III} complexes. This is also consistent with the ac susceptibility and hysteresis measurements. Moreover, only the magnetic relaxation in the complexes **1Er** and **2Er** can occur by the second excited state.[5d,15] The calculated magnetic easy axis of Er^{III} complexes

This journal is © the Partner Organisations 2016

Inorg. Chem. Front., 2016, **3**, 828–835 | 831
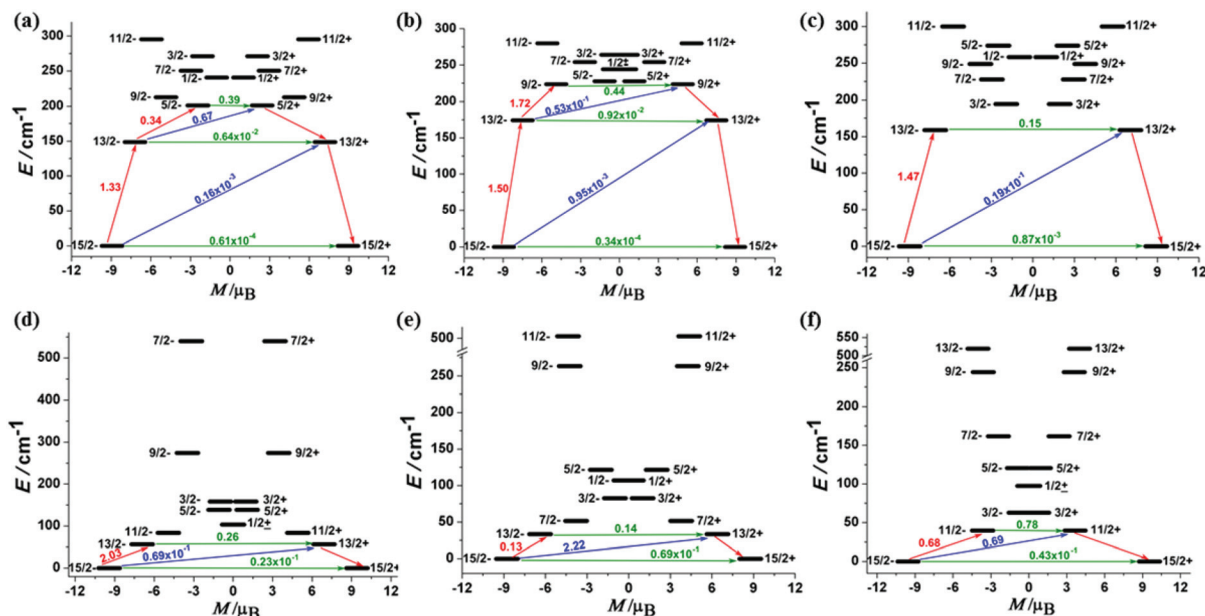
Fig. 5 The magnetization blocking barriers in complexes **1Er–6Dy**, represented by (a)–(f). The thick black lines represent Kramer's doublets as a function of their magnetic moment along the magnetic axis. The green lines correspond to diagonal quantum tunneling of magnetization (QTM), the blue lines represent the off-diagonal relaxation process. The numbers at each arrow stand for the mean absolute value of the corresponding matrix element of the transition magnetic moment.

further confirmed that the sandwich type geometry is preferable for the prolate type Er^{III} ion possessing SIM properties (Fig. S18†). On the contrary, the easy axis of Dy^{III} complexes is not perpendicular to the COT ring as in the case of the Er^{III} complexes (Fig. S18†), as the equatorial ligand field is not suitable to stabilize the Ising type oblate ground state of the Dy^{III} ion.

Unprecedented frozen magnetization

The $\chi_m T$ rising observed for **1Er** and **2Er** at 12 or 6 K has no precedent. As the rising occurs around their T_B, the magnetization may be "frozen" below a certain temperature. Two independent measurements were carried out: (a) the magnetization of **1Er** was measured upon cooling; (b) the sample was firstly cooled to 2 K under 1 kOe dc field, and then the magnetization was measured upon warming. At each data point, the measurement was delayed for a certain time before the data were recorded. During the cooling down experiment, the $\chi_m T$ value decreases smoothly and no peak was observed (Fig. S19†), while in the warming up experiment, the $\chi_m T$ rising was observed (Fig. 6). When the delay time is 2 s, a distinct peak was observed at about 6.3 K. The $\chi_m T$ rising becomes less pronounced when increasing the delay time. When the delay time is up to 7200 s, the $\chi_m T$ rising can be ignored (Fig. 6). These results indicate that a long delay time is needed to let the system relax to equilibrium. Indeed, the magnetization equilibrium at 2 K can only be reached by delaying as long as 10 hours (Fig. S20†). This is probably due to the poor coupling of the spin system and the phonon bath.[16] These results
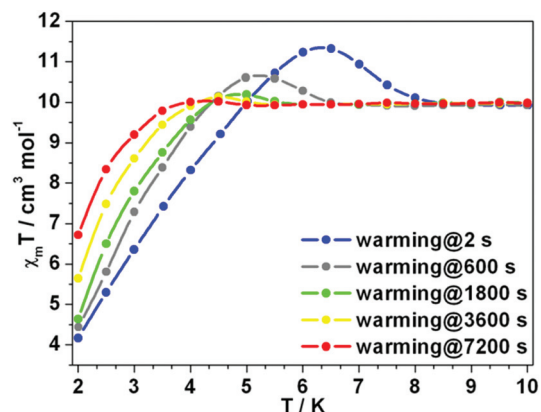
Fig. 6 Variable-temperature dc susceptibility data of **1Er**. Changing the interval time can make the unexpected rising disappear.

indicate that the observed $\chi_m T$ rising is not due to the long range ordering, but the non-equilibrium of magnetization.

Conclusions

In summary, sandwich type lanthanide organometallic complexes $[(C_5H_5BR)Ln(COT)]$ were successfully synthesized, the erbium complexes are SIMs while the dysprosium ones are not, and the magnetic properties of the erbium complexes are strongly influenced by the substituent on the boron atom. Using poorer electron donating boratabenzene $[C_5H_5BR]^-$ (R = H or Me) instead of carbon aromatic anions, such as Cp*

832 | *Inorg. Chem. Front.*, 2016, **3**, 828–835

This journal is © the Partner Organisations 2016

and COT, results in erbium SIMs with a higher effective energy barrier. It is also noteworthy that the blocking temperature of $[(C_5H_5BH)Er(COT)]$ is higher than that of $[(Cp^*)Er(COT)]$. This study experimentally demonstrated that utilizing poorer electron donors—boratabenzenes—decreases the electronic interaction between the 4f electrons and aromatic electrons of ligands along the uniaxial direction, and enhances the uniaxial magnetic anisotropy. Therefore, this study not only disclosed a new application of the boratabenzene metal complexes but also provided a practical guideline for the design and synthesis of erbium SIMs with better performance. Further studies following this guideline are actually ongoing.

Experimental

General methods

The synthesis of air and/or moisture sensitive compounds was carried out under an atmosphere of argon using Schlenk techniques or in a nitrogen filled glovebox. Toluene, hexane, and THF were dried over a Na/K alloy, transferred under vacuum, and stored in the glovebox. $[(COT)LnCl(THF)](Ln = Er, Dy, Y)$,[17] $Li(C_5H_5BH)$,[10e] and $Li(C_5H_5BNEt_2)$[10d] were prepared according to literature procedures. [1H] NMR and [13C] NMR spectra were recorded on a VARIAN Mercury 400 MHz spectrometer at 400 MHz and 100 MHz, respectively. [11B] NMR spectra were recorded on an Agilent 600 MHz spectrometer at 193 MHz. All chemical shifts were reported in δ units with reference to the residual solvent resonance of the deuterated solvents for proton and carbon chemical shifts, and to external $BF_3 \cdot OEt_2$ for boron chemical shifts. Elemental analysis was performed by the Analytical Laboratory of Shanghai Institute of Organic Chemistry. ICP analysis was performed by the Analytical Instrumentation Center of Peking University.

$Li(C_5H_5BCH_3)$. $Li(C_5H_5BCH_3)$[18] was prepared by using Fu's method.[19] A solution of $C_5H_5BPMe_3$ (972 mg, 6.39 mmol) in 30 mL of ether was added by 3.0 M MeLi solution in DEM (DEM = diethoxymethane) (2.1 mL, 6.30 mmol) at −30 °C under stirring, and then the reaction mixture was gradually warmed to room temperature. After stirring for one hour at room temperature, the volatiles of the reaction mixture were removed *in vacuo*. The residue was washed with 2 × 10 mL of hexane and dried *in vacuo* to give $Li(C_5H_5BCH_3)$ as a pale yellow solid (594 mg, 96% yield). [1H] NMR (400 MHz, THF-d_8, 25 °C): δ(ppm) 7.06 (t, J_{H-H} = 8.4 Hz, 2H, 3-/5-H), 6.25 (d, J_{H-H} = 10.4 Hz, 2H, 2-/6-H), 5.96 (t, J_{H-H} = 6.8 Hz, 1H, 4-H), 0.47 (s, 3H, CH_3).

$[(C_5H_5BH)Er(COT)]$ (1Er). $[(COT)ErCl(THF)]$ (100 mg, 0.264 mmol) and $Li(C_5H_5BH)$ (22 mg, 0.262 mmol) were mixed in 4 mL of THF at −35 °C, and the reaction mixture was stirred overnight at room temperature. The solvent was removed *in vacuo*, and the residue was extracted with 5 mL of toluene. The extraction was concentrated to *ca.* 2 mL and kept at −35 °C to give **1Er** as orange crystals (52 mg, 57% yield). Anal. Calcd (%) for $C_{13}H_{14}BEr$: C, 44.83, H, 4.05. Found: C, 44.49, H, 4.17.

$[(C_5H_5BMe)Er(COT)]$ (2Er). $[(COT)ErCl(THF)]$ (100 mg, 0.264 mmol) and $Li(C_5H_5BCH_3)$ (26 mg, 0.265 mmol) were mixed in 4 mL of THF at −35 °C, and the reaction mixture was stirred overnight at room temperature. The solvent was removed *in vacuo*, and the residue was extracted with 5 mL of toluene. Evaporation of this filtrate *in vacuo* left an orange oil, which was extracted with 10 mL of hexane. The hexane extraction was concentrated to *ca.* 4 mL and kept at −35 °C to give **2Er** as orange crystals (53 mg, 55% yield). Anal. Calcd (%) for $C_{14}H_{16}BEr$: C, 46.41, H, 4.45. Found: C, 46.23, H, 4.42.

$[(C_5H_5BNEt_2)Er(COT)]$ (3Er). Following the procedure described for **1Er**. The reaction of $[(COT)ErCl(THF)]$ (100 mg, 0.264 mmol) with $Li(C_5H_5BNEt_2)$ (40 mg, 0.258 mmol) gave **3Er** as orange crystals (61 mg, 56% yield). Anal. Calcd (%) for $C_{17}H_{23}BErN$: C, 48.68, H, 5.53, N, 3.34. Found: C, 48.46, H, 5.46, N, 3.27.

$[(C_5H_5BH)Dy(COT)]$ (4Dy). Following the procedure described for **1Er**. The reaction of $[(COT)DyCl(THF)]$ (100 mg, 0.267 mmol) with $Li(C_5H_5BH)$ (23 mg, 0.274 mmol) gave **4Dy** as yellow crystals (51 mg, 55% yield). Anal. Calcd (%) for $C_{13}H_{14}BDy$: C, 45.45, H, 4.11. Found: C, 44.91, H, 4.16.

$[(C_5H_5BMe)Dy(COT)]$ (5Dy). Following the procedure described for **2Er**. The reaction of $[(COT)DyCl(THF)]$ (100 mg, 0.267 mmol) with $Li(C_5H_5BMe)$ (26 mg, 0.265 mmol) gave **5Dy** as yellow crystals (40 mg, 42% yield). Anal. Calcd (%) for $C_{14}H_{16}BDy$: C, 47.02, H, 4.51. Found: C, 46.97, H, 4.66.

$[(C_5H_5BNEt_2)Dy(COT)]$ (6Dy). Following the procedure described for **1Er**. The reaction of $[(COT)DyCl(THF)]$ (100 mg, 0.267 mmol) with $Li(C_5H_5BNEt_2)$ (41 mg, 0.264 mmol) gave **6Dy** as yellow crystals (59 mg, 54% yield). Anal. Calcd (%) for $C_{17}H_{23}BDyN$: C, 49.24, H, 5.59, N, 3.38. Found: C, 49.00, H, 5.60, N, 3.33.

$[(C_5H_5BNEt_2)Y(COT)]$ (7Y). Following the procedure described for **1Er**. The reaction of $[(COT)YCl(THF)]$ (171 mg, 0.569 mmol) with $Li(C_5H_5BNEt_2)$ (88 mg, 0.569 mmol) gave **7Y** as yellow crystals (85 mg, 44% yield). [1H] NMR (400 MHz, C_6D_6, 25 °C): δ = 6.52 (t, $^3J_{H-H}$ = 7.2 Hz, 2H, 3-/5-H of Bz), 6.35 (s, 8H, H of COD), 5.35 (d, $^3J_{H-H}$ = 10.4 Hz, 2H, 2-/6-H of Bz), 5.02 (t, $^3J_{H-H}$ = 6.8 Hz, 1H, 4-H of Bz), 2.94 (bs, 4H, NCH_2), 1.07 (t, $^3J_{H-H}$ = 6.8 Hz, 6H, NCH$_2$CH_3). [13C] NMR (100 MHz, C_6D_6, 25 °C): δ = 135.3, 112.2, 100.9 (Bz-C), 94.03 (COD-C), 43.2 (NCH$_2$CH$_3$), 15.8 (NCH$_2$CH_3). [11B] NMR (193 MHz, C_6D_6, 25 °C): δ = 30.1. Anal. Calcd (%) for $C_{17}H_{23}BYN$: C, 59.86, H, 6.80, N, 4.11. Found: C, 60.16, H, 6.93, N, 3.94.

X-ray crystallography

Suitable single crystals of **1Er–7Y** (CCDC 1416019–1416025) were mounted under a nitrogen atmosphere on a glass fiber at low temperature, and data collection was performed on a Bruker APEX2 diffractometer with graphite-monochromated Mo K$_\alpha$ radiation (λ = 0.71073 Å). The SMART program package was used to determine the unit cell parameters. The absorption correction was applied using SADABS. The structures were solved by direct methods and refined on F^2 by full-matrix least-squares techniques with anisotropic thermal parameters for nonhydrogen atoms. The hydrogen atoms were placed at

This journal is © the Partner Organisations 2016

Inorg. Chem. Front., 2016, **3**, 828–835 | 833

calculated positions and were included in the structure calculation. All calculations were carried out using the SHELXL-97 program. The software used is listed in ref. 20. Crystallographic data and refinement for **1Er–7Y** are listed in Table S1.†

Magnetic measurements

Samples were fixed with eicosane to avoid moving during the measurement and sealed in the glass tube to avoid reaction with moisture and oxygen. Direct current susceptibility and alternative current susceptibility with frequencies ranging from 1 to 997 Hz were performed on a Quantum Design MPMS XL-5 SQUID magnetometer on polycrystalline samples. The alternative current susceptibility measurement with frequencies ranging from 100 to 10 000 Hz was performed on Quantum Design PPMS on polycrystalline samples. All dc susceptibilities were corrected for diamagnetic contribution from the sample holder, and eicosane and diamagnetic contributions from the molecule using Pascal's constants.

Ab initio calculations

All calculations were done with CASSCF/RASSI/SINGLE_ANISO implanted in the MOLCAS 7.8 package. All calculations used the complete structures of **1Er–6Dy**. Using the SINGLE_ANISO program we obtained their magnetic properties. Complete-active-space self-consistent field (CASSCF) calculations on the complete structures of complexes **1Er–6Dy** on the basis of X-ray determined geometry have been carried out with the MOLCAS 7.8 program package. For CASSCF calculations, the basis sets for all atoms are atomic natural orbitals from the MOLCAS ANO-RCC library: ANO-RCC-VTZP for the Er^{III} or Dy^{III} ion, VTZ for close C and B, VDZ for the distant atoms. The calculations employed the second order Douglas–Kroll–Hess Hamiltonian, where scalar relativistic contractions were taken into account in the basis set and the spin–orbit coupling was handled separately in the restricted active space state interaction (RASSI-SO) procedure. The active electrons in 7 active spaces include all the f electrons (CAS(11 in 7) for complexes **1Er–3Er** and CAS(9 in 7) for complexes **4Dy–6Dy**) in the CASSCF calculation. To exclude all the doubts we calculated all the roots in the active space. We have mixed the maximum number of spin-free states which was possible with our hardware (all from 35 quadruplets and all from 112 doublets for three Er^{III} fragments, all from 21 sextets, 128 from 224 quadruplets and 130 from 490 doublets for three Dy^{III} fragments).

Acknowledgements

Notes and references

1 (*a*) A. Caneschi, D. Gatteschi, R. Sessoli, A. L. Barra, L. C. Brunel and M. Guillot, *J. Am. Chem. Soc.*, 1991, **113**, 5873; (*b*) R. Sessoli, H. L. Tsai, A. R. Schake, S. Wang, J. B. Vincent, K. Folting, D. Gatteschi, G. Christou and D. N. Hendrickson, *J. Am. Chem. Soc.*, 1993, **115**, 1804; (*c*) R. Sessoli, D. Gatteschi, A. Caneschi and M. A. Novak, *Nature*, 1993, **365**, 141; (*d*) D. Gatteschi, A. Caneschi, L. Pardi and R. Sessoli, *Science*, 1994, **265**, 1054.

2 (*a*) A. J. Tasiopoulos, A. Vinslava, W. Wernsdorfer, K. A. Abboud and G. Christou, *Angew. Chem., Int. Ed.*, 2004, **43**, 2117; (*b*) A. M. Ako, I. J. Hewitt, V. Mereacre, R. Clérac, W. Wernsdorfer, C. E. Anson and A. K. Powell, *Angew. Chem., Int. Ed.*, 2006, **45**, 4926; (*c*) C. J. Milios, A. Vinslava, W. Wernsdorfer, S. Moggach, S. Parsons, S. P. Perlepes, G. Christou and E. K. Brechin, *J. Am. Chem. Soc.*, 2007, **129**, 2754.

3 (*a*) J. A. Jones, *Science*, 1998, **280**, 229; (*b*) W. Wernsdorfer, *C. R. Chim.*, 2008, **11**, 1086; (*c*) W. Wernsdorfer and R. Sessoli, *Science*, 1999, **284**, 133; (*d*) Y. F. Zhang, N. Lorente, K. Katoh, Y. Yoshida, M. Yamashita and B. K. Breedlove, *Nat. Commun.*, 2011, **2**, 217; (*e*) L. E. Rosaleny and A. Gaita-Arino, *Inorg. Chem. Front.*, 2016, **3**, 61.

4 (*a*) N. Ishikawa, M. Sugita, T. Ishikawa, S.-y. Koshihara and Y. Kaizu, *J. Am. Chem. Soc.*, 2003, **125**, 8694; (*b*) N. Ishikawa, M. Sugita, T. Ishikawa, S.-y. Koshihara and Y. Kaizu, *J. Phys. Chem. B*, 2004, **108**, 11265; (*c*) N. Ishikawa, M. Sugita and W. Wernsdorfer, *Angew. Chem., Int. Ed.*, 2005, **44**, 2931; (*d*) S.-D. Jiang, B.-W. Wang, G. Su, Z.-M. Wang and S. Gao, *Angew. Chem., Int. Ed.*, 2010, **49**, 7448; (*e*) M. A. AlDamen, J. M. Clemente-Juan, E. Coronado, C. Martí-Gastaldo and A. Gaita-Ariño, *J. Am. Chem. Soc.*, 2008, **130**, 8874; (*f*) J.-L. Liu, Y.-C. Chen, Y.-Z. Zheng, W.-Q. Lin, L. Ungur, W. Wernsdorfer, L. F. Chibotaru and M.-L. Tong, *Chem. Sci.*, 2013, **4**, 3310; (*g*) Y. Bi, Y.-N. Guo, L. Zhao, Y. Guo, S.-Y. Lin, S.-D. Jiang, J. Tang, B.-W. Wang and S. Gao, *Chem. – Eur. J.*, 2011, **17**, 12476; (*h*) M. Jeletic, P.-H. Lin, J. J. Le Roy, I. Korobkov, S. I. Gorelsky and M. Murugesu, *J. Am. Chem. Soc.*, 2011, **133**, 19286; (*i*) S. Demir, J. M. Zadrozny and J. R. Long, *Chem. – Eur. J.*, 2014, **20**, 9524; (*j*) W.-B. Sun, B. Yan, Y.-Q. Zhang, B.-W. Wang, Z.-M. Wang, J.-H. Jia and S. Gao, *Inorg. Chem. Front.*, 2014, **1**, 503; (*k*) P. Zhang, L. Zhang, C. Wang, S. Xue, S.-Y. Lin and J. Tang, *J. Am. Chem. Soc.*, 2014, **136**, 4484; (*l*) P. Martín-Ramos, M. Ramos Silva, J. T. Coutinho, L. C. J. Pereira, P. Chamorro-Posada and J. Martín-Gil, *Eur. J. Inorg. Chem.*, 2014, **2014**, 511; (*m*) W.-B. Sun, B. Yan, Y.-Q. Zhang, B.-W. Wang, Z.-M. Wang, J.-H. Jia and S. Gao, *Inorg. Chem. Front.*, 2014, **1**, 503; (*n*) K. Soussi, J. Jung, F. Pointillart, B. Le Guennic, B. Lefeuvre, S. Golhen, O. Cador, Y. Guyot, O. Maury and L. Ouahab, *Inorg. Chem. Front*, 2015, **2**, 1105.

834 | *Inorg. Chem. Front.*, 2016, **3**, 828–835

This journal is © the Partner Organisations 2016

5 (*a*) S.-D. Jiang, B.-W. Wang, H.-L. Sun, Z.-M. Wang and S. Gao, *J. Am. Chem. Soc.*, 2011, **133**, 4730; (*b*) K. R. Meihaus and J. R. Long, *J. Am. Chem. Soc.*, 2013, **135**, 17952; (*c*) J. J. Le Roy, I. Korobkov and M. Murugesu, *Chem. Commun.*, 2014, **50**, 1602; (*d*) L. Ungur, J. J. Le Roy, I. Korobkov, M. Murugesu and L. F. Chibotaru, *Angew. Chem., Int. Ed.*, 2014, **53**, 4413.

6 G. E. Herberich, G. Greiss and H. F. Heil, *Angew. Chem., Int. Ed. Engl.*, 1970, **9**, 805.

7 A. J. Ashe III and P. Shu, *J. Am. Chem. Soc.*, 1971, **93**, 1804.

8 For reviews, see: (*a*) G. E. Herberich and H. Ohst, *Adv. Organomet. Chem.*, 1986, **25**, 199; (*b*) A. J. Ashe III, S. Al-Ahmad and X. G. Fang, *J. Organomet. Chem.*, 1999, **581**, 92; (*c*) G. C. Fu, *Adv. Organomet. Chem.*, 2001, **47**, 101; (*d*) P. Cui and Y. F. Chen, *Coord. Chem. Rev.*, DOI: 10.1016/j.ccr.2015.07.014.

9 (*a*) G. E. Herberich, U. Englert, A. Fischer, J. H. Ni and A. Schmitz, *Organometallics*, 1999, **18**, 5496; (*b*) M. A. Putzer, J. S. Rogers and G. C. Bazan, *J. Am. Chem. Soc.*, 1999, **121**, 8112; (*c*) A. J. Ashe III, S. Al-Ahmad, X. D. Fang and J. W. Kampf, *Organometallics*, 2001, **20**, 468; (*d*) N. Auvray, T. S. Basu Baul, P. Braunstein, P. Croizat, U. Englert, G. E. Herberich and R. Welter, *Dalton Trans.*, 2006, 2950; (*e*) A. Languérand, S. S. Barnes, G. Bélanger-Chabot, L. Maron, P. Berrouard, P. Audet and F. G. Fontaine, *Angew. Chem., Int. Ed.*, 2009, **48**, 6695; (*f*) G. Bélanger-Chabot, P. Rioux, L. Maron and F. G. Fontaine, *Chem. Commun.*, 2010, **46**, 6816; (*g*) P. Frank, R. A. Lalancette and F. Jäkle, *Chem. – Eur. J.*, 2011, **17**, 11280; (*h*) A. Glöckner, P. Cui, Y. F. Chen, C. G. Daniliuc, P. G. Jones and M. Tamm, *New J. Chem.*, 2012, **36**, 1392; (*i*) B. B. Macha, J. Boudreau, L. Maron, T. Maris and F. Fontaine, *Organometallics*, 2012, **31**, 6428; (*j*) A. Mushtaq, W. Bi, M.-A. Légaré and F.-G. Fontaine, *Organometallics*, 2014, **33**, 3173.

10 (*a*) G. C. Bazan, G. Rodriguez, A. J. Ashe III, S. Al-Ahmad and C. Müller, *J. Am. Chem. Soc.*, 1996, **118**, 2291; (*b*) G. C. Bazan, G. Rodriguez, A. J. Ashe III, S. Al-Ahmad and J. W. Kampf, *Organometallics*, 1997, **16**, 2492; (*c*) J. S. Rogers, X. H. Bu and G. C. Bazan, *J. Am. Chem. Soc.*, 2000, **122**, 730; (*d*) Y. Y. Yuan, Y. F. Chen, G. Y. Li and W. Xia, *Organometallics*, 2008, **27**, 6307; (*e*) Y. Y. Yuan, X. F. Wang, Y. X. Li, L. Y. Fan, X. Xu, Y. F. Chen, G. Y. Li and W. Xia, *Organometallics*, 2011, **30**, 4330; (*f*) X. F. Wang, W. J. Peng, P. Cui, X. B. Leng, W. Xia and Y. F. Chen, *Organometallics*, 2013, **32**, 6166; (*g*) E. L. Lu, Y. Y. Yuan, Y. F. Chen and W. Xia, *ACS Catal.*, 2013, **3**, 521.

11 O. Kahn, *Molecular Magnetism*, VCH Publishers, New York, Weinheim, 1993.

12 S. K. Singh, T. Gupta and G. Rajaraman, *Inorg. Chem.*, 2014, **53**, 10835.

13 F. Aquilante, L. De Vico, N. Ferré, G. Ghigo, P.-å. Malmqvist, P. Neogrády, T. B. Pedersen, M. Pitoňák, M. Reiher, B. O. Roos, L. Serrano-Andrés, M. Urban, V. Veryazov and R. Lindh, *J. Comput. Chem.*, 2010, **31**, 224.

14 L. Ungur, M. Thewissen, J.-P. Costes, W. Wernsdorfer and L. F. Chibotaru, *Inorg. Chem.*, 2013, **52**, 6328.

15 R. J. Blagg, L. Ungur, F. Tuna, J. Speak, P. Comar, D. Collison, W. Wernsdorfer, E. J. L. McInnes, L. F. Chibotaru and R. E. P. Winpenny, *Nat. Chem.*, 2013, **5**, 673.

16 (*a*) R. Orbach, *Spin-Lattice Relaxation in Rare-Earth Salts*, 1961, vol. 264; (*b*) P. L. Scott and C. D. Jeffries, *Phys. Rev.*, 1962, **127**, 32; (*c*) M.-E. Boulon, G. Cucinotta, S.-S. Liu, S.-D. Jiang, L. Ungur, L. F. Chibotaru, S. Gao and R. Sessoli, *Chem. – Eur. J.*, 2013, **19**, 13726.

17 (*a*) K. O. Hodgson, F. Mares, D. F. Starks and A. Streitwieser, *J. Am. Chem. Soc.*, 1973, **95**, 8650; (*b*) A. L. Wayda, *Organometallics*, 1983, **2**, 565.

18 G. E. Herberich, B. Schmidt and U. Englert, *Organometallics*, 1995, **14**, 471.

19 S. Qiao, D. A. Hoic and G. C. Fu, *J. Am. Chem. Soc.*, 1996, **118**, 6329.

20 (*a*) G. M. Sheldrick, *SADABS, An Empirical Absorption Correction Program for Area Detector Data*, University of Göttingen, Göttingen, Germany, 1996; (*b*) G. M. Sheldrick, *SHELXS-97 and SHELXL-97*, University of Göttingen, Göttingen, Germany, 1997; (*c*) *SMART Version 5.628*, Bruker AXS Inc., Madison, WI, 2002; (*d*) *SAINT+ Version 6.22a*, Bruker AXS Inc., Madison, WI, 2002; (*e*) *SHELXTL NT/2000, Version 6.1*, Bruker AXS Inc., Madison, WI, 2002.

This journal is © the Partner Organisations 2016

Inorg. Chem. Front., 2016, **3**, 828–835 | **835**